AMERICAN SOCIETY FOR MICROBIOLOGY | mBio®

RESEARCH ARTICLE

Targeting the Fusion Process of SARS-CoV-2 Infection by Small Molecule Inhibitors

Seung Bum Park,[a] Parker Irvin,[a] Zongyi Hu,[a] Mohsin Khan,[a] Xin Hu,[b] Qiru Zeng,[c] Catherine Chen,[b] Miao Xu,[b] Madeleine Leek,[a] Ruochen Zang,[c] James Brett Case,[d] Wei Zheng,[b] Siyuan Ding,[c] T. Jake Liang[a]*

[a]Liver Diseases Branch, NIDDK, NIH, Bethesda, Maryland, USA
[b]Division of Pre-Clinical Innovations, NCATS, NIH, Rockville, Maryland, USA
[c]Department of Molecular Microbiology, Washington University School of Medicine, St. Louis, Missouri, USA
[d]Department of Medicine, Division of Infectious Diseases, Washington University School of Medicine, St. Louis, Missouri, USA

ABSTRACT Coronavirus disease 2019 (COVID-19), caused by severe acute respiratory syndrome coronavirus 2 (SARS-CoV-2), has become a serious threat to global public health, underscoring the urgency of developing effective therapies. Therapeutics and, more specifically, direct-acting antiviral development are still very much in their infancy. Here, we report that two hepatitis C virus (HCV) fusion inhibitors identified in our previous study, dichlorcyclizine and fluoxazolevir, broadly block human coronavirus entry into various cell types. Both compounds were effective against various human-pathogenic CoVs in multiple assays based on vesicular stomatitis virus (VSV) pseudotyped with the spike protein and spike-mediated syncytium formation. The antiviral effects were confirmed in SARS-CoV-2 infection systems. These compounds were equally effective against recently emerged variants, including the delta variant. Cross-linking experiments and structural modeling suggest that the compounds bind to a hydrophobic pocket near the fusion peptide of S protein, consistent with their potential mechanism of action as fusion inhibitors. In summary, these fusion inhibitors have broad-spectrum antiviral activities and may be promising leads for treatment of SARS-CoV-2, its variants, and other pathogenic CoVs.

IMPORTANCE SARS-CoV-2 is an enveloped virus that requires membrane fusion for entry into host cells. Since the fusion process is relatively conserved among enveloped viruses, we tested our HCV fusion inhibitors, dichlorcyclizine and fluoxazolevir, against SARS-CoV-2. We performed *in vitro* assays and demonstrated their effective antiviral activity against SARS-CoV-2 and its variants. Cross-linking experiments and structural modeling suggest that the compounds bind to a hydrophobic pocket in spike protein to exert their inhibitory effect on the fusion step. These data suggest that both dichlorcyclizine and fluoxazolevir are promising candidates for further development as treatment for SARS-CoV-2.

KEYWORDS SARS-CoV-2, COVID-19, viral entry, viral fusion, fusion inhibitor, broad-spectrum antiviral, antiviral agents, coronavirus, structural modeling, viral variants

Severe acute respiratory syndrome coronavirus 2 (SARS-CoV-2) is an enveloped, single-stranded, positive-sense RNA virus with a genome size of ~30 kb. It belongs to the family *Coronaviridae* (1) and is the pathogen responsible for the coronavirus disease 2019 (COVID-19) pandemic. In addition to SARS-CoV-2, several other strains of coronaviruses are highly pathogenic in humans. For example, SARS-CoV and Middle East respiratory syndrome coronavirus (MERS-CoV) have caused widespread infections in 2002 and 2012, respectively. No vaccines or effective drugs for either SARS-CoV or MERS-CoV are available, and despite significant efforts, treatment options for COVID-19 are also limited, even with many drug candidates currently and previously undergoing clinical trials. So far, the only small molecule direct-acting antiviral that has received approval by the U.S. Food and Drug Administration (FDA) is remdesivir (Veklury), an inhibitor of the viral RNA-dependent RNA polymerase. Remdesivir was

Editor Thomas Shenk, Princeton University

Address correspondence to T. Jake Liang, jakel@bdg10.niddk.nih.gov.
*Present address: T. Jake Liang, Liver Diseases Branch, NIDDK, NIH, Bethesda, Maryland, USA.
The authors declare no conflict of interest.
This article is a direct contribution from T. Jake Liang, a Fellow of the American Academy of Microbiology, who arranged for and secured reviews by Thomas Baumert, University of Strasbourg, Hopitaux Universitaires de Strasbourg, and Jeffrey Glenn, Stanford University School of Medicine.
Received 2 November 2021
Accepted 23 November 2021
Published 11 January 2022

initially developed for the treatment of Ebola virus infection and recently recognized as a promising broad-spectrum antiviral against RNA viruses (2, 3). Remdesivir can shorten recovery time but does not improve mortality in those with serious COVID-19 (4, 5), underscoring the urgent need for development of effective antivirals.

Given the challenges in developing reliable high-throughput screening of SARS-CoV-2 inhibitors in infectious system, we focused on the development of viral entry inhibitors, a process that can be accurately assessed by currently available methods without a high-containment facility.

The SARS-CoV-2 spike (S) glycoprotein is required for viral entry into host cells. The S protein has two functional domains, S1 and S2 (6). S1 contains a receptor-binding domain (RBD), and S2 drives the fusion of viral and host membrane once S1 binds to its host cell receptor, angiotensin-converting enzyme 2 (ACE2). After S1-ACE2 binding, S is cleaved by cellular proteases, such as transmembrane protease serine subtype 2 (TMPRSS2) or endosomal cathepsins, to expose the fusion peptide that apposes viral and host cell membranes for fusion (7, 8). Coronaviruses can deliver their genomes to the host cytoplasm by either direct fusion with the plasma membrane (pH independent) or utilizing the host cell's endocytic pathway (pH dependent) (9). Viral entry, therefore, can be blocked by not only directly inhibiting S-ACE2 binding but also by interfering with fusion by targeting the S fusion peptide, cellular proteases, or other factors critical for the endocytic route.

We previously identified several hepatitis C virus (HCV) entry inhibitors targeting the fusion step (10–15). Since the fusion process is relatively conserved among enveloped viruses, we aimed to test several of our HCV fusion inhibitors against SARS-CoV-2 (16, 17). We selected promising candidates dichlorcyclizine (DCCZ) and fluoxazolevir for further characterization. Here, we report the antiviral effects and putative mechanisms of these compounds against various pathogenic human CoVs. Both dichlorcyclizine and fluoxazolevir are highly effective in *in vitro* assays, including SARS-CoV-2 S pseudotyped particles, chimeric vesicular stomatitis virus (VSV), and cell-cell fusion assays. The results were confirmed by using SARS-CoV-2 infection systems *in vitro*. Both compounds were active against recently described SARS-CoV-2 variants, including the delta variant, in various virological assays (18–35). Thus, dichlorcyclizine and fluoxazolevir are promising candidates for further development and could be important in stopping the spread of and treating those infected by SARS-CoV-2 as well as future emerging coronaviruses.

RESULTS

Dichlorcyclizine and fluoxazolevir inhibit human CoV S-mediated infection. We previously reported the identification and development of two fusion inhibitors for HCV: dichlorcyclizine and fluoxazolevir (10–15). As the fusion process is relatively conserved (16, 17), we hypothesized that these two probes also may be active against other viruses. We tested these inhibitors against SARS-CoV, SARS-CoV-2, and MERS-CoV, together with (*S*)-chlorcyclizine [(*S*)-CCZ], an approved antihistamine drug that is related to dichlorcyclizine (36) and other recently described SARS-CoV-2 entry inhibitors, such as chloroquine (37), camostat (38), and E-64d (38). For *in vitro* experiments, pseudotyped VSVs harboring SARS-CoV S (SARS-Spp), SARS-CoV-2 S (SARS2-Spp), and MERS-CoV S (MERS-Spp) were generated to test the efficacy and define the mechanism of the inhibitors. We tested three cell lines, African green monkey kidney cells (MA104), human embryonic kidney cells expressing ACE2 (293ACE2), and human hepatoma cells (Huh7), which are susceptible to SARS-CoV-2 infection (39). All three cell lines were susceptible to infection by each of the pseudotyped viruses, with the exception of 293ACE2 cells that was not susceptible to MERS-Spp, because this cell line lacks the MERS-CoV receptor DPP4 (40). (*S*)-CCZ, dichlorcyclizine, and fluoxazolevir suppressed SARS-Spp and SARS2-Spp entry in MA104 (Fig. 1a), 293ACE2 (Fig. 1b), and Huh7 (Fig. 1c) cells with 50% effective concentration (EC_{50}) values in the range of single-digit micromolar concentrations (Table 1). The three compounds also exhibited efficient inhibition of MERS-CoV-Spp entry in MA104 and Huh7 (see Fig. S1 in the supplemental material). Chloroquine and E-64d (cathepsin B/L inhibitor) but not camostat (TMPRSS2 inhibitor)

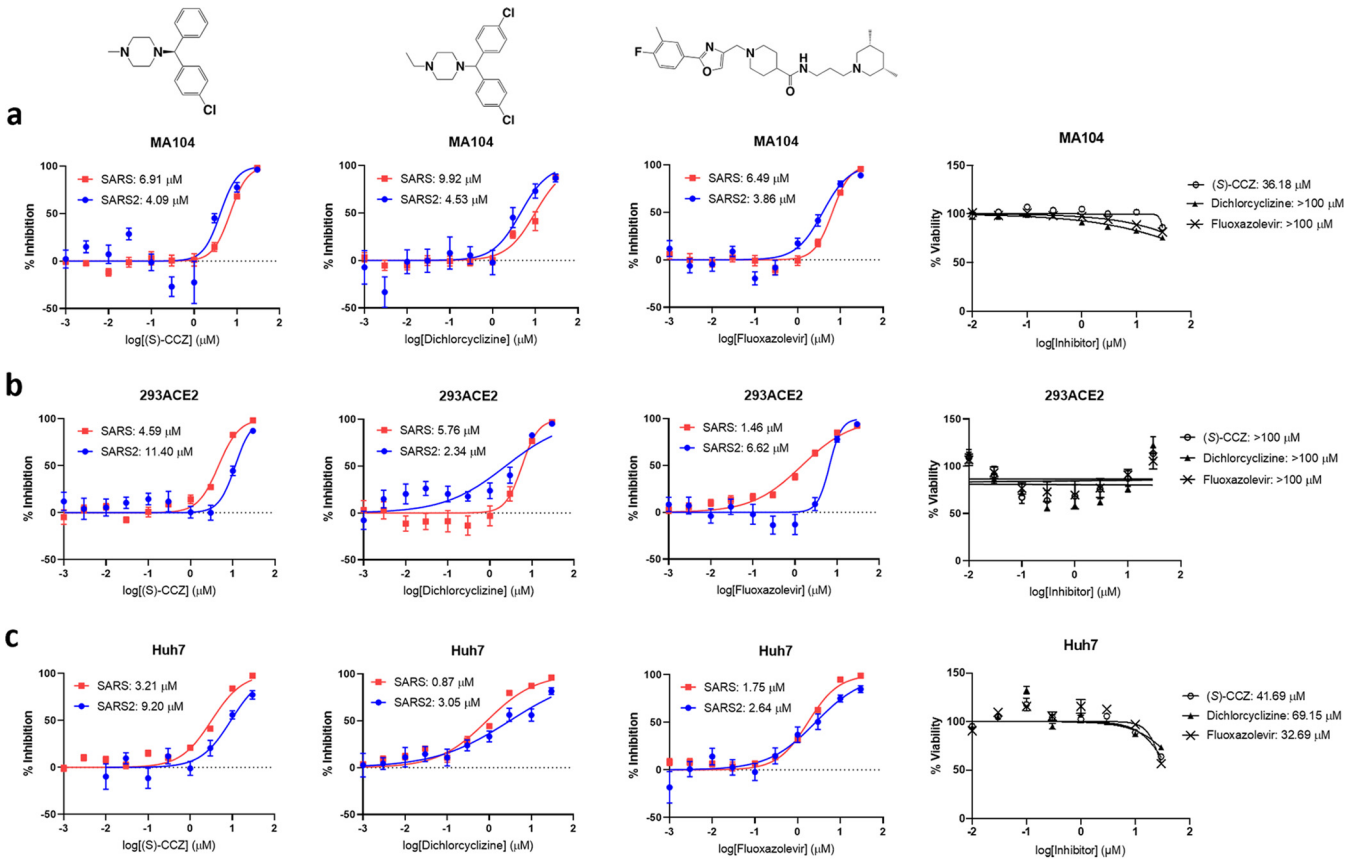

FIG 1 (*S*)-CCZ, dichlorcyclizine, and fluoxazolevir inhibit human CoV S-mediated infection. The chemical structures of (*S*)-CCZ, dichlorcyclizine, and fluoxazolevir are shown on the top. SARS-CoV and SARS-CoV-2 pseudotyped virus infection and cytotoxicity (right) assays were performed in MA104 (a), 293ACE2 (b), and Huh7 (c) cells with (*S*)-CCZ, dichlorcyclizine, and fluoxazolevir, with dimethyl sulfoxide (DMSO) as a control (see Materials and Methods). Luminescent signals were measured using a POLARstar Omega plate reader. EC_{50} and CC_{50} values were calculated using Prism 7 software. Each data point is presented as mean values ± standard errors of the means (n = 6 to 8 biological independent replicates). All results are representative of three independent experiments.

inhibited SARS-Spp and SARS2-Spp entry in all three cell lines (Fig. S1). Similarly, chloroquine and E-64d but not camostat reduced MERS-Spp entry for MA104 and Huh7 cells (Fig. S1).

To test whether these compounds are not toxic, a cytotoxicity assay was performed. In MA104 and 293ACE2 cell lines, no cytotoxicity was detected for all compounds (50% cytotoxic concentration [CC_{50}], >100 μM), while (*S*)-CCZ, dichlorcyclizine, fluoxazolevir, and chloroquine exhibited some cytotoxicity in Huh7 cells at high concentrations (CC_{50} > 30 μM) (Fig. 1). In addition, we tested VSV-Gpp entry in MA104, Huh7, and 293ACE2 cells with the above-described 6 inhibitors. Chloroquine showed strong inhibition, whereas fluoxazolevir exhibited minimal and (*S*)-CCZ and dichlorcyclizine displayed no inhibition (Fig. S2a and b), suggesting some selectivity of these compounds against coronavirus spike proteins over VSV glycoprotein.

Next, we tested these compounds in recombinant chimeric vesicular stomatitis virus (rVSV-SARS-CoV-2-S-GFP) that has been genetically engineered to express green fluorescent protein (GFP) and SARS-CoV-2 S protein in place of its native envelope glycoprotein, G protein (39). This reporter virus is capable of replicating and propagating in cells susceptible to SARS-CoV-2. Both dichlorcyclizine and fluoxazolevir as well as chloroquine inhibited rVSV-SARS-CoV-2-S-GFP infection of MA104 cells (Fig. 2a). Quantification of the GFP signals was used to generate a dose-dependent curve with EC_{50} values within a single-digit micromolar range (Fig. 2b). VSV RNA levels of the infected cells were quantified by reverse transcription-quantitative PCR (RT-qPCR) and showed a similar dose-response curve (Fig. 2c).

Dichlorcyclizine and fluoxazolevir inhibit wild-type SARS-CoV-2 infection. To confirm whether these compounds are active against infectious live virus, we tested them in three

TABLE 1 Summary of EC_{50} and CC_{50} values for SARS-CoV-2

Compound and cell	EC_{50} (μM)	EC_{90}	CC_{50}
(*S*)-CCZ			
MA104	4.09	11.14	36.18
293ACE2	11.40	ND[a]	>100
Huh7	9.20	ND	41.69
Dichlorcyclizine			
MA104	4.53	ND	>100
293ACE2	2.34	ND	>100
Huh7	3.05	ND	69.15
Fluoxazolevir			
MA104	3.86	18.5	>100
293ACE2	6.62	13.64	>100
Huh7	2.64	ND	32.64
Chloroquine			
MA104	7.65	32.28	>100
293ACE2	2.07	30.18	>100
Huh7	4.38	ND	37.54
Camostat			
MA104	>100	ND	>100
293ACE2	>100	ND	>100
Huh7	>100	ND	>100
E-64d			
MA104	0.14	3.07	>100
293ACE2	0.21	0.68	>100
Huh7	0.26	9.29	>100

[a]ND, not determined on account of either not reaching 90% inhibition with the highest concentration of compound or substandard dose-response curve.

infectious SARS-CoV-2 systems, one using a standard wild-type SARS-CoV-2 strain (2019-nCoV/USA-WA1/2020 strain) and two recombinant infectious viruses expressing a mNeonGreen reporter (icSARS-CoV-2mNG) (41) or Nanoluciferase (SARS-CoV-2-NLuc). We measured the antiviral activity of dichlorcyclizine and fluoxazolevir against SARS-CoV-2 using remdesivir as a control (Fig. 2d to f). Both dichlorcyclizine and fluoxazolevir showed inhibition of icSARS-CoV-2mNG and SARS-CoV-2-NLuc infections with EC_{50} values in the single-digit micromolar range (Fig. 2d and e). In wild-type SARS-CoV-2 infection cell culture, viral replication was measured by RT-qPCR of SARS-CoV-2 RNA. Both dichlorcyclizine and fluoxazolevir showed dose-dependent inhibition with up to 2-log suppression of viral RNA levels (Fig. 2f), which was less than that of remdesivir (up to 3 logs).

Inhibition of SARS-CoV-2 spike variants by dichlorcyclizine and fluoxazolevir. Recently various SARS-CoV-2 variants have emerged in various parts of the world and appear to be more infectious and virulent and perhaps less susceptible to vaccine-induced immunity (18–24, 31–35). Thus, we generated pseudotyped VSVs harboring SARS-CoV-2 S with mutations reported in the alpha, beta, delta, and other variants, either in combination or individually (25–27). First, to estimate the infectivity of S pseudotyped viruses of alpha, beta, and delta variants and those with individual mutations in our system, we quantified the genome copy numbers of the pseudotyped viruses by using quantitative PCR primers in the VSV L gene and then measured infectivity by using the same multiplicity of infection (based on genome copy number). Additional mutants harboring individual L452R, S477N, N679S, and Q677H mutations that have been reported in other variants were also tested for infectivity. All mutants were similarly infectious with less than a 2-fold difference (Fig. 3a).

Wild-type, alpha, beta, and delta pseudoviruses showed similar susceptibility to both dichlorcyclizine and fluoxazolevir with similar EC_{50} values (Fig. 3b). In addition, we tested our compounds against various individual mutations in the spike protein of these and other reported variants, such as N439K, Y453F, E484K, N501Y, D614G, and P681H. Chloroquine and E-64d were also tested against these variants. Like the above-described

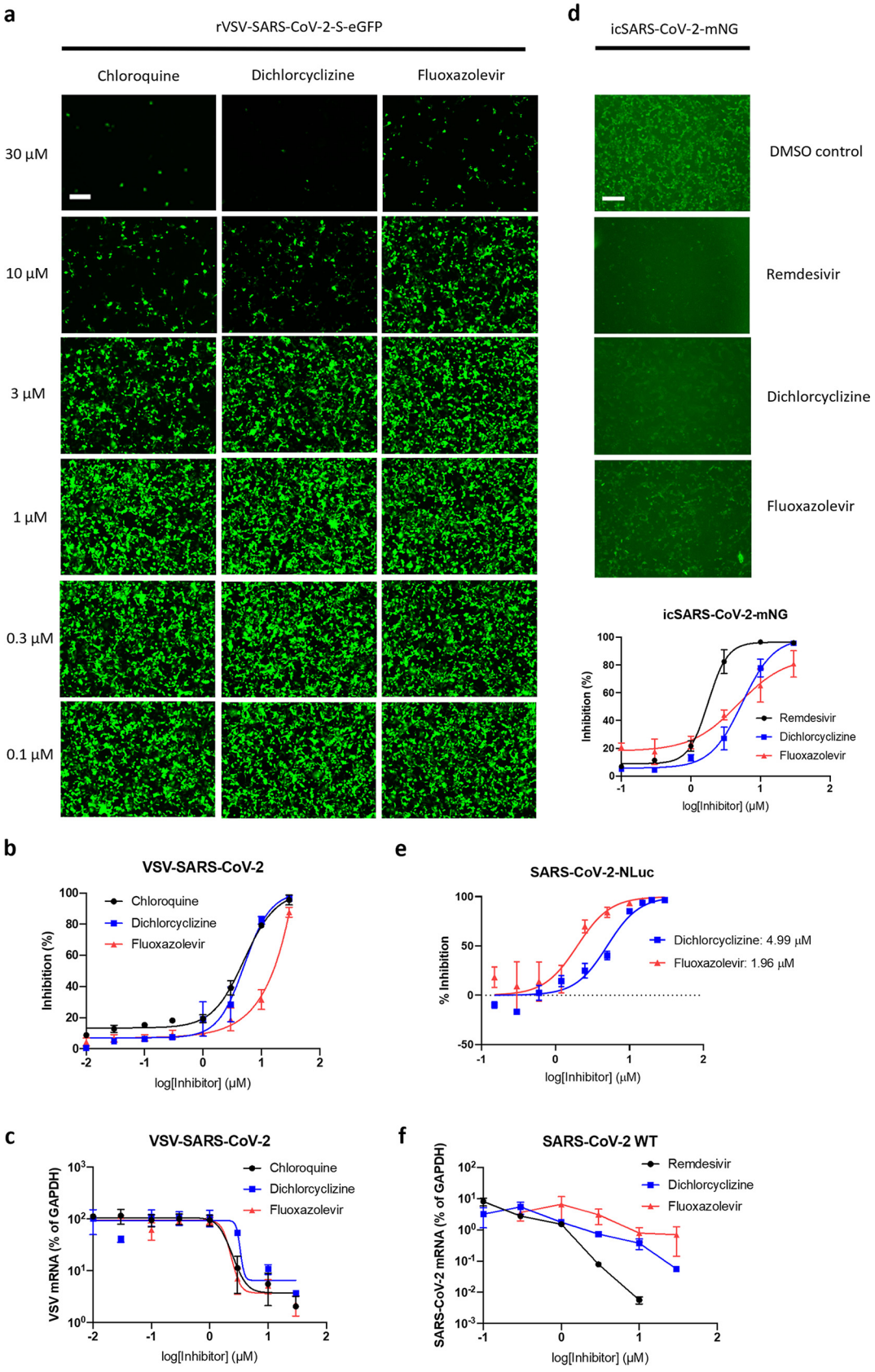

FIG 2 Dichlorcyclizine and fluoxazolevir suppress wild-type SARS-CoV-2 infection. (a to c) MA104 cells were treated with chloroquine, dichlorcyclizine, and fluoxazolevir at the indicated concentrations for 1 h and infected with rVSV-SARS-CoV-2-S-eGFP

(Continued on next page)

results, the mutants harboring individual mutations also showed similar EC_{50} values with minor variations (<2-fold) against all compounds (Fig. 3c).

Next, we tested isolates of infectious alpha and beta variants against our compounds. Both dichlorcyclizine and fluoxazolevir showed similar inhibition against wild-type, alpha, and beta SARS-CoV-2 variants in Vero E6 cells with and without TMPRSS2 expression (Fig. 3d).

Dichlorcyclizine and fluoxazolevir do not block SARS-CoV-2 binding to cells. To investigate whether dichlorcyclizine and fluoxazolevir interfere with the initial attachment of virus to the cells, a viral binding assay was performed. Cells were first incubated with the SARS2-Spp in the presence of the compounds at 4°C for binding and then raised to 37°C for entry. Cell-associated viral RNA was then isolated and quantified. Heparan sulfate, anti-S1 (RBD) antibody, and E-64d were also tested in the assay. Previous studies showed that SARS-CoV-2 binds with high affinity to certain glycosaminoglycans of cell surface proteoglycan, such as heparan sulfate, which likely mediates the initial attachment of virus to the cells (42, 43). Heparan sulfate significantly inhibited the binding of SARS-CoV-2 virus to cells, whereas E-64d, dichlorcyclizine, and fluoxazolevir had little or no effect on viral binding (Fig. 4a). Anti-S1 (RBD) antibody that blocks the interaction of RBD with ACE2 inhibited SARS-CoV-2-S pseudotyped virus infection efficiently (Fig. S2c) but did not affect much viral binding (Fig. 4a). This finding is consistent with previous reports that heparan sulfate proteoglycan (HSPG) binds to the S1 in a distinct domain from the ACE2-binding RBD, and interaction between the RBD and ACE2 likely occurs after the initial attachment of the virus to cells via HSPG (42, 43).

Dichlorcyclizine and fluoxazolevir inhibit a late entry stage of SARS-CoV-2 infection. To further elucidate the mechanism of action for dichlorcyclizine and fluoxazolevir, a time of addition assay was performed (14). Neutralizing antibody targeting the S1 domain of spike and E-64d were used as controls. In order to allow binding and synchronized entry, SARS2-Spp was added from −2 h to 0 h at 4°C for allowing binding of the viruses to the host cell surface and to synchronize entry. The temperature then was increased from 4°C to 37°C for internalization of the viruses. Compounds were added at different time points for 2 h to determine the timing of inhibition during entry. Anti-S antibody showed inhibition when present from −2 h to 0 h, but dichlorcyclizine and fluoxazolevir displayed minimal inhibition in this time period (Fig. 4b). In contrast, when compounds were present from 0 h to 2 h and 0.5 h to 2.5 h, both dichlorcyclizine and fluoxazolevir showed potent inhibition, whereas anti-S antibody had little effect, indicating that the compounds target a late stage of viral entry (Fig. 4b). E-64d displayed inhibition during binding (−2 to 0 h), early (0 to 2 h, 0.5 to 2.5 h), and middle (1 to 3 h) entry time points (Fig. 4b). E-64d, while supposedly blocking viral entry at the fusion step like our two compounds, is an irreversible inhibitor (44) and, thus, would be expected to also show inhibition when it was added earlier (−2 to 0 h).

Dichlorcyclizine and fluoxazolevir block SARS-CoV-2 spike protein-mediated cell-cell fusion. SARS-CoV, SARS-CoV-2, and MERS-CoV can enter cells via either plasma membrane or endosomal membrane fusion, depending on the availability of cell surface-associated proteases, such as TMPRSS2, and other undetermined factors (7, 38). To assess SARS-CoV-2 S protein-mediated plasma membrane fusion, we developed two distinct cell-cell fusion assays: the SmBit-LgBit (split luciferase) and GFP-RFP systems (Fig. S3). Briefly, donor cells (HeLa cells) express S-SmBit or S-GFP fusion protein. HeLa cells are not susceptible to SARS-CoV-2 infection because they do not express ACE2 (39) and, thus, do not undergo self-fusion. Confocal microscopy was performed to demonstrate the expression

FIG 2 Legend (Continued)
(multiplicity of infection, 3). At 24 hpi, cells were fixed and the GFP signals were captured and quantified using a Typhoon biomolecular imager (a) and then plotted as percentage of inhibition (b). Scale bar, 100 μm. (c) Alternatively, VSV-N RNA levels were measured by RT-qPCR and normalized to glyceraldehyde-3-phosphate dehydrogenase (GAPDH) expression. (d) Vero E6 cells were treated with remdesivir (10 μM), dichlorcyclizine (10 μM), fluoxazolevir (30 μM), and DMSO as a control and infected with icSARS-CoV-2-mNeonGreen (multiplicity of infection, 0.5). At 24 hpi, cells were fixed and the mNeonGreen signals were captured and quantified using a Typhoon biomolecular imager (top) and then plotted as percentage of inhibition (bottom). Scale bar, 100 μm. (e) Vero E6 cells were infected with SARS-CoV-2-NLuc at a multiplicity of infection of 0.1. At 16 hpi, luminescent signals were measured by using a POLARstar Omega plate reader. EC_{50} was calculated using Prism 7 software. (f) Infection was performed with wild-type SARS-CoV-2 and treated with the compounds. At 24 hpi, SARS-CoV-2 RNA levels were measured by RT-qPCR using primers in the N gene and normalized to GAPDH expression. All results are representative of three independent experiments.

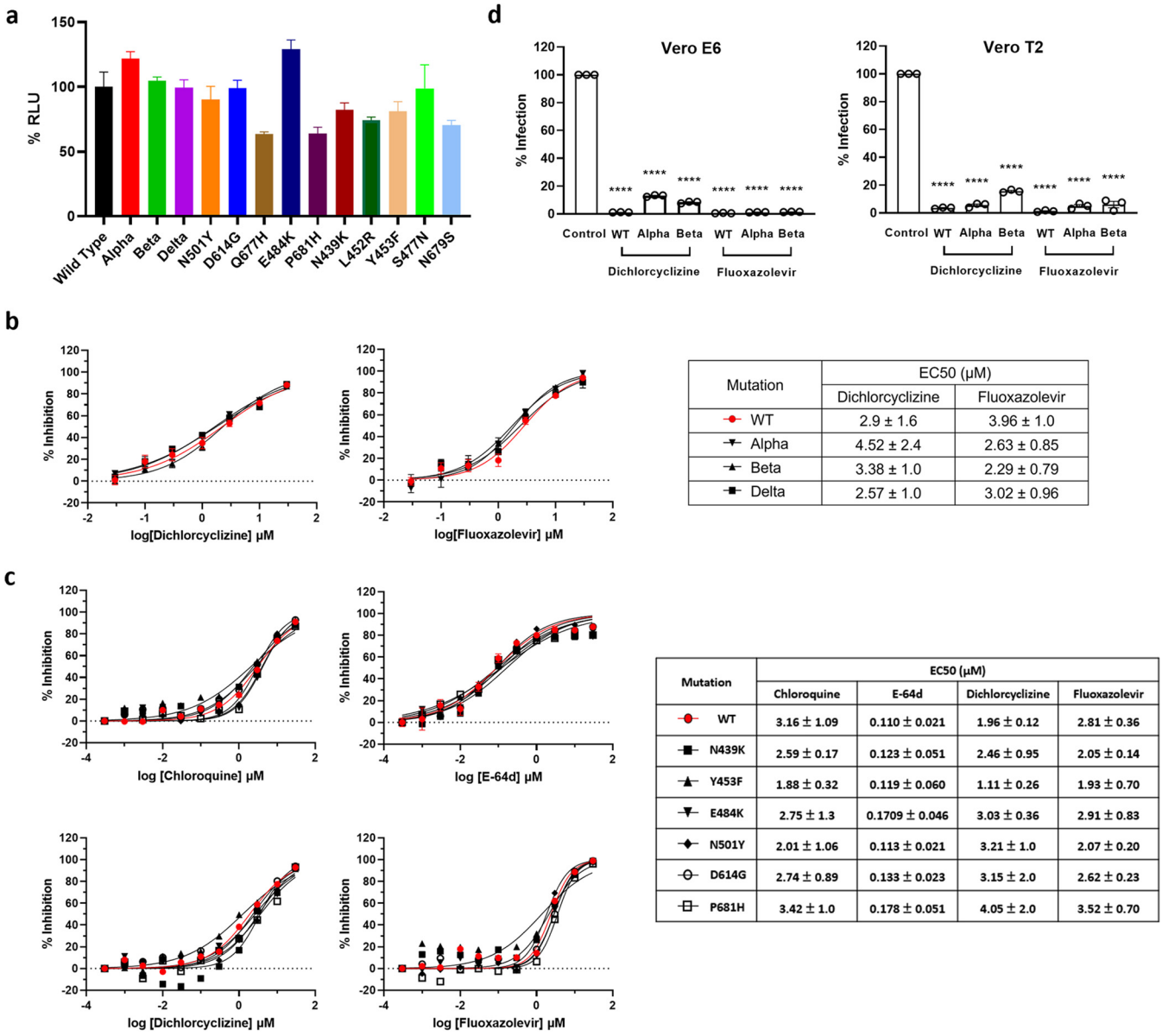

Mutation	EC50 (μM)	
	Dichlorcyclizine	Fluoxazolevir
WT	2.9 ± 1.6	3.96 ± 1.0
Alpha	4.52 ± 2.4	2.63 ± 0.85
Beta	3.38 ± 1.0	2.29 ± 0.79
Delta	2.57 ± 1.0	3.02 ± 0.96

Mutation	EC50 (μM)			
	Chloroquine	E-64d	Dichlorcyclizine	Fluoxazolevir
WT	3.16 ± 1.09	0.110 ± 0.021	1.96 ± 0.12	2.81 ± 0.36
N439K	2.59 ± 0.17	0.123 ± 0.051	2.46 ± 0.95	2.05 ± 0.14
Y453F	1.88 ± 0.32	0.119 ± 0.060	1.11 ± 0.26	1.93 ± 0.70
E484K	2.75 ± 1.3	0.1709 ± 0.046	3.03 ± 0.36	2.91 ± 0.83
N501Y	2.01 ± 1.06	0.113 ± 0.021	3.21 ± 1.0	2.07 ± 0.20
D614G	2.74 ± 0.89	0.133 ± 0.023	3.15 ± 2.0	2.62 ± 0.23
P681H	3.42 ± 1.0	0.178 ± 0.051	4.05 ± 2.0	3.52 ± 0.70

FIG 3 Efficacy of dichlorcyclizine and fluoxazolevir against SARS-CoV-2 variants. (a) VSV-SARS-CoV-2-S pseudotyped virus containing N439K, L452R, Y453F, S477N, E484K, N501Y, D614G, Q677H, N679S, or P681H mutation was generated. VSV L mRNA levels were measured to calculate genome copy numbers per volume of pseudotyped VSV stock. The cells were then infected with the same multiplicity of infection, and luminescent signals were measured using a POLARstar Omega plate reader. Each data point is presented as mean values ± SEM (n = 6 to 8 biological independent replicates). (b) VSV-SARS-CoV-2-S pseudotyped viruses containing mutations appearing in alpha, beta, and delta variants were generated and tested against dichlorcyclizine and fluoxazolevir in Huh7 cells. Luminescent signals were measured using a POLARstar Omega plate reader 24 h after infection. EC_{50} values are calculated using Prism 7 software and shown in the table on the right. Each data point is presented as mean values ± SEM (n = 6 to 8 biological independent replicates). (c) VSV-SARS-CoV-2-S pseudotyped viruses containing N439K, Y453F, E484K, N501Y, D614G, or P681H mutations were tested against (*S*)-CCZ, dichlorcyclizine, and fluoxazolevir in Huh7 cells. Luminescent signals were measured using a POLARstar Omega plate reader. EC_{50} values are calculated using Prism 7 software and shown in the table on the right. Each data point is presented as mean values ± SEM (n = 6 to 8 biological independent replicates). (d) Vero E6 and Vero T2 cells were infected with wild-type, alpha, and beta variants at a multiplicity of infection of 0.1 with or without 10 μM the compounds. At 16 h postinfection, SARS-CoV-2 RNA was measured using primers targeting N. Relative levels of the viral genome were calculated using the GAPDH gene as a normalization control. The data are presented as means ± SD (three independent replicates). All results are representative of three independent experiments.

of spike protein in the donor cells (HeLa) (Fig. S4). The expressed S protein was stained by antibody to either S1 or S2 domain and displayed both cytoplasmic and cell membrane staining. Recipient cells are 293ACE2 cells expressing LgBit or RFP. After successful fusion between donor and recipient cells, interaction between SmBit and LgBit emits luminescent signals (Fig. S3a), and colocalization between GFP and red fluorescent protein (RFP) generates yellow fluorescence signal (Fig. S3b).

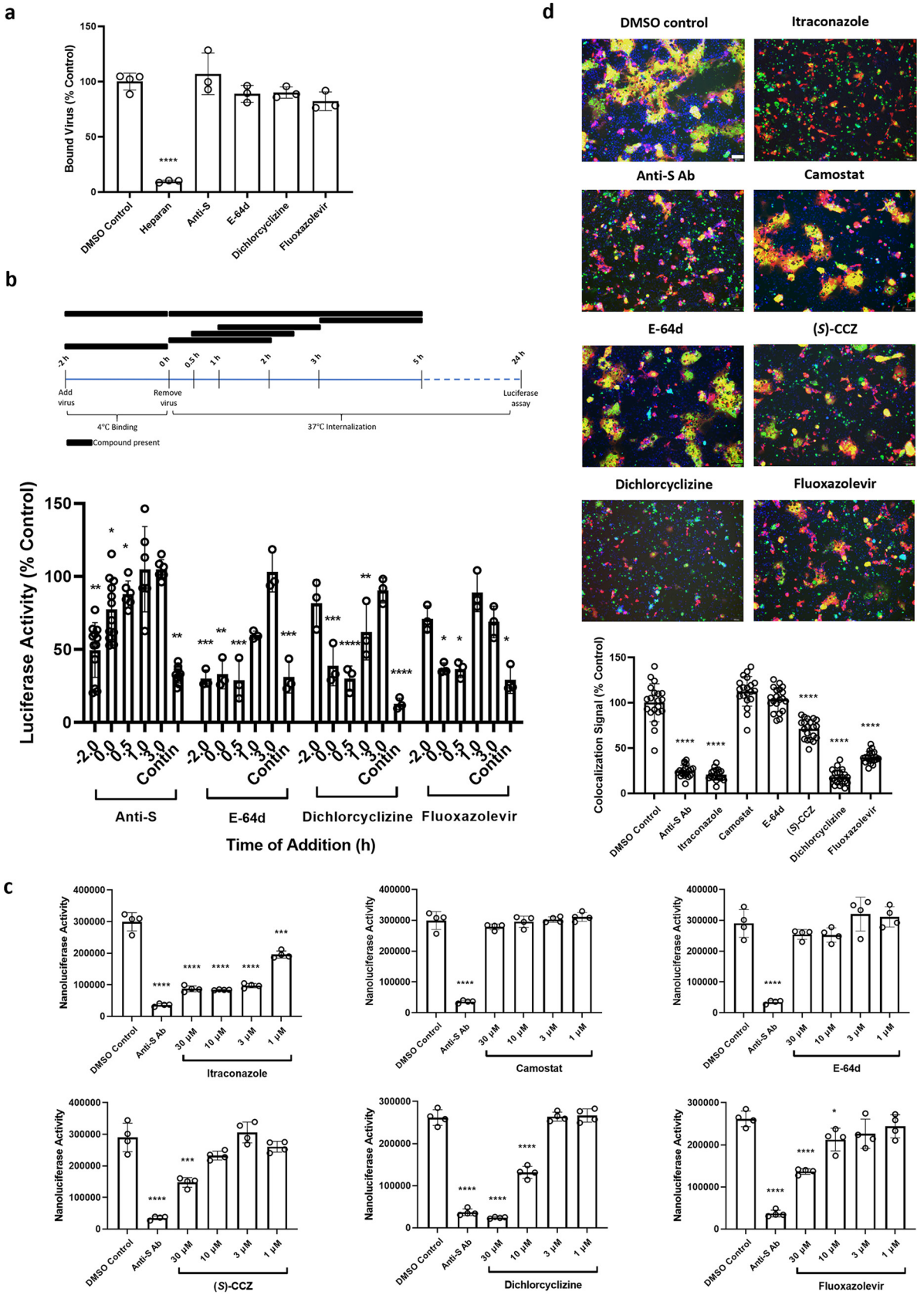

FIG 4 Time-of-addition and cell-cell fusion assays. (a) Huh7 cells were chilled to 4°C following incubation with ice-cold pseudotyped virus and compounds at 4°C for 2 h to allow binding but not internalization. The cells then were washed twice with plain medium and once

(Continued on next page)

To confirm that the fusion event is mediated specifically by the binding of S to its receptor, ACE2, we tested wild-type cells that do not express SmBit, LgBit, GFP, or RFP. We also tested donor cells expressing GFP-SmBit without the S protein as a negative control (Fig. S3c to e). In addition, an anti-S antibody capable of neutralizing SARS-CoV-2 S-mediated infection was used to show that the fusion can be blocked (Fig. 4c and d). Both cell-cell fusion assays model the plasma membrane fusion route and provide mechanistic insight into the action of our compounds.

(*S*)-CCZ, dichlorcyclizine, and fluoxazolevir inhibited donor-recipient fusion events in the SmBit-LgBit system (Fig. 4c). Notably, dichlorcyclizine exhibited potent inhibition at levels similar to the positive control, itraconazole (45, 46) (Fig. 4c). Camostat and E-64d did not suppress fusion events, probably because TMPRSS2 is not expressed on 293ACE2 cells and endosomal cathepsins are not involved in cell-cell surface fusion (Fig. 4c). An anti-S antibody was also effective in blocking fusion.

In the GFP-RFP system of the cell-cell fusion assay, (*S*)-CCZ, dichlorcyclizine, and fluoxazolevir showed inhibition of fusion (Fig. 4d). The colocalization signals were quantified and are shown in the lower panel of Fig. 4d. Dichlorcyclizine exhibited strong inhibition similar to that of itraconazole. As in the SmBit-LgBit system, camostat and E-64d did not decrease fusion signals (Fig. 4d). Taken together, (*S*)-CCZ, dichlorcyclizine, and fluoxazolevir likely inhibit plasma membrane fusion mediated by SARS-CoV-2 S, with dichlorcyclizine being the most potent compound.

Absence of drug resistance-associated mutations by *in vitro* selection. Antibody resistance-associated mutations in the SARS-CoV-2 S protein, particularly in the receptor binding domain, can emerge readily both *in vitro* and *in vivo* (47–49). Thus, the potential emergence of drug resistance-associated mutations for any direct-acting antivirals developed against SARS-CoV-2 would be a concern. The locations of these viral mutations would also provide valuable insight into the mechanism of action of these antivirals (15). To address this question, we tested the recombinant chimeric VSV (rVSV-SARS-CoV-2-S-GFP) used previously to generate antibody resistance mutations (50) to select for drug resistance-associated mutations against dichlorcyclizine. This virus was serially passaged in increasing concentrations of dichlorcyclizine, and any passaged viral isolates showing putative resistance to dichlorcyclizine ($>$2-fold increase in EC_{50}) would be sequenced for any S protein mutations (Fig. S5). After 25 serial passages, we did not observe any clear emergence of drug-resistant viral isolates.

CCZ-diazirine probe specifically cross-links SARS-CoV-2 spike protein. To identify the molecular target for chlorcyclizine, we used a previously reported photoaffinity probe CCZ-DB (15). First, CCZ-DB, when tested against VSV-SARS-CoV-2-S pseudotyped virus, was active in a dose-dependent manner, with EC_{50} values of 12.92 μM (Fig. 5a). The DB-Ctrl control probe was inactive. We previously reported the binding of CCZ to a putative fusion peptide pocket in HCV E1 protein (15). Here, we hypothesized that CCZ binds to the appropriate coun-

FIG 4 Legend (Continued)
with PBS to remove unbound virus. The VSV L gene mRNA level was measured by RT-qPCR. The concentrations used for this experiment are following: heparin sodium porcine mucosa (25 μM), anti-S1 antibody (15 μg/ml), E-64d (15 μM), dichlorcyclizine (15 μM), and fluoxazolevir (15 μM). (b) Time of addition assay was performed with anti-S antibody, E-64d, dichlorcyclizine, and fluoxazolevir (see Materials and Methods). Huh7 cells were chilled to 4°C and then incubated with ice-cold pseudotyped virus at 4°C for 2 h to allow binding but not internalization. After binding, cells were incubated at 37°C overnight to allow for internalization. Compounds were added during binding ($-$2 to 0 h) or at early (0 to 2 h, 0.5 to 2.5 h), middle (1 to 3 h), or late (3 to 5 h) entry time points postbinding. For the continuous treatment groups, compounds were added during the 4°C binding stage ($-$2 to 0 h) and added for an additional 5 h after washing and temperature shift to 37°C (0 to 5 h). For all other treatment groups, compounds were washed off 2 h after addition. Cells were lysed 24 h postinfection and were measured for their luciferase activity. Luminescent signals were measured using a POLARstar Omega plate reader. The results are representative of three independent experiments. (c) Cell-cell fusion assays were performed with (*S*)-CCZ, dichlorcyclizine, fluoxazolevir, and other control compounds (see Materials and Methods). The S-SmBit-transfected donor (HeLa) and the LgBit-transfected recipient (293ACE2) cell mixture were treated with four different concentrations (30 μM, 10 μM, 3 μM, and 1 μM) of the above-described compounds and DMSO as a control for 48 h. Anti-S antibody (Ab) was used as a positive control. After incubation, luminescent signals were measured using a POLARstar Omega plate reader. Each data point is presented as mean values $\pm$ SEM (n = 4 biological independent replicates). (d) These compounds at 30 μM were used to treat S-GFP-transfected donor (HeLa) and the RFP-transfected recipient (293ACE2) cell mixture for 48 h. Anti-S antibody was used as a control. Representative fields are shown. For quantification, 20 fields were randomly selected from 4 replicates to measure the fused cells under a CellSens fluorescence microscope. ImageJ was used to quantify colocalization signals. For statistical comparison, adjusted P values are shown (versus DMSO control, *, $P < 0.05$; **, $P < 0.01$; ***, $P < 0.001$; ****, $P < 0.0001$). All results are representative of three independent experiments. Scale bar, 100 μm.

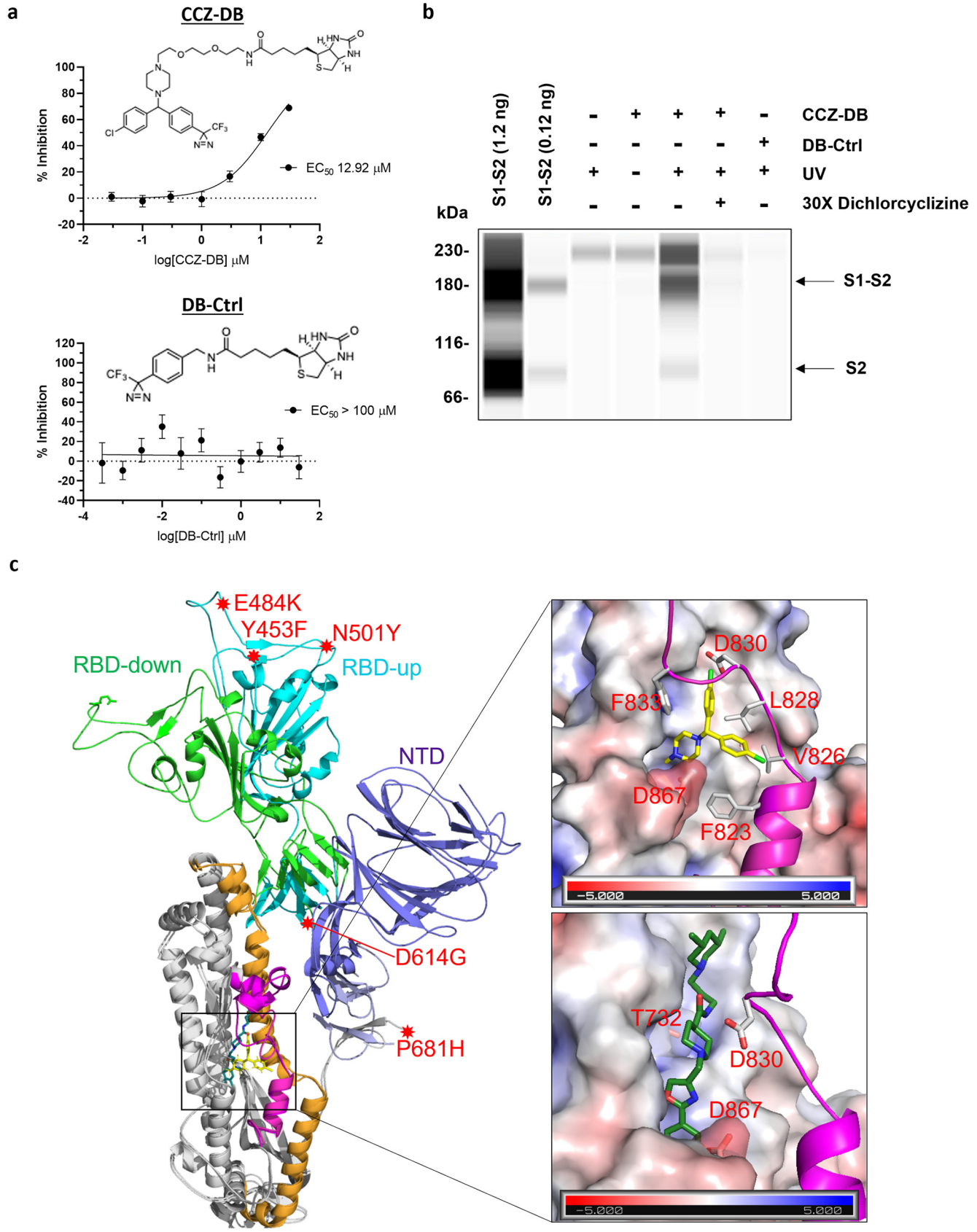

FIG 5 Antiviral mechanism of dichlorcyclizine and fluoxazolevir against SARS-CoV-2. (a) Structures and dose-response curves of CCZ-DB and DB-Ctrl. CCZ-DB was active in inhibiting pseudotyped VSVs harboring SARS-CoV-2 S, with an EC_{50} of 12.92 μM. The DB-Ctrl has the diazirine-biotin moieties but was not

(Continued on next page)

terpart of HCV E1 in SARS-CoV-2, which is the fusion peptide of spike protein. Using the photoaffinity probe CCZ-DB, we showed its direct binding to the recombinant SARS-CoV-2 S1-S2 protein only after UV-activated cross-linking (Fig. 5b). DB-Ctrl was used as a control. The binding shows specificity because a 30-fold excess of dichlorcyclizine could outcompete the cross-linking of the probe to the spike protein.

Association of dichlorcyclizine and fluoxazolevir with S fusion peptide by molecular modeling. Dichlorcyclizine and fluoxazolevir have been shown to bind near the putative fusion peptide of HCV (10–15). We reasoned they also bind to a similar domain in the S protein of SARS-CoV-2. The fusion peptide (FP) (amino acid 815 to 852) of SARS-CoV-2 mediates viral fusion and is highly flexible, with a well-defined N-terminal short helix followed by a disordered C-terminal structure in the prefusion structure of S (6, 51, 52) (Fig. 5c). The C-terminal FP, also referred to as the fusion peptide-proximal region (FPPR), can form a more packed and defined structure in the S trimer complex that exhibits an RBD-down conformation (51) (Fig. 5c). Analysis of these available structures showed a well-defined hydrophobic pocket formed by the FP helix region and the adjacent HR1 domain (Fig. 5c). The hydrophobic pocket is partially covered by the structured FPPR in the RBD-down conformation, while it is rather open and extended to a hydrophobic groove along the adjacent HR1 helix and the FP disordered structure in the RBD-up conformation.

We modeled the flexible FP loop and performed molecular dynamic simulations to examine the dynamics and conformational changes of the FP in an open and intermediate conformation, which is directly associated with its functional role in the membrane fusion process. Docking of dichlorcyclizine and fluoxazolevir to these ensembles of structural conformations showed that these small molecules are accommodated well in the FP hydrophobic pocket (Fig. 5c and Fig. S6). DCCZ can dock into both open and close conformations of the fusion peptide. Fluoxazolevir, because of its extended structure, can dock into the open conformation but is partially blocked by the structured FPPR in the RBD-down conformation. It is interesting that the well-described variant carrying the D614G mutation has a more RBD-up conformation of the S protein (31), which may be more accessible to inhibitors like fluoxazolevir.

For DCCZ, an H-bond is formed between the piperazine N with D867, similar to the key H-bonding interaction in HCV (15). Another interaction can occur with F833 from the FP, which points into the pocket and forms π-π stacking interaction with the phenyl group of DCCZ, while the chlorine can form halogen bonding with FP residue D830. A nearby FP residue, F823, can also form π-π stacking interaction with the other phenyl group of DCCZ, and V826 and L828 can contribute to π-alkyl interaction with both phenyl groups (Fig. 5c). Fluoxazolevir fits into the same pocket with potential hydrogen bonds between N of the oxazole and the same D867 residue (Fig. 5c). Other potential hydrogen bonds can also form between N of the central piperidine and T732 as well as between N of the central amide and the D830.

The structures of the S2 domains of S proteins of SARS-CoV, SARS-CoV-2, and MERS-CoV share major similarities (24). The fusion peptides of both SARS-CoV and MERS-CoV are also highly flexible and typically disordered in the S protein structure and can form a similar hydrophobic pocket. Docking of DCCZ and fluoxazolevir to the pocket showed the same binding mode. Interestingly, the key interaction residues D867 and F833 in SARS-CoV-2 are highly conserved in SARS-CoV and MERS-CoV.

FIG 5 Legend (Continued)
active against pseudotyped VSVs harboring SARS-CoV-2 S. (b) Purified recombinant S1-S2 protein was incubated with CCZ-DB at room temperature for 2 h, subjected to UV cross-linking, and then purified by Neutravidin beads followed by Western blotting with anti-S2 antibody. Recombinant S1-S2 protein was included as a reference. In one sample, a 30-fold higher concentration of dichlorcyclizine was added to the CCZ-DB cross-linking condition to test competition between dichlorcyclizine and CCZ. (c) Structural modeling of SARS-CoV-2 S protein and fusion peptide. The three-dimensional structure of SARS-CoV-2 S protein trimer was used for docking analysis of dichlorcyclizine and fluoxazolevir. The monomeric S protomer with the down (green) or up (turquoise) receptor binding domain (RBD) conformation and the N-terminal domain (NTD) are depicted in the middle. The fusion peptide (magenta) and heptad repeat 1 (HR1) (brown) of S2 are shown. The locations of the variant amino acids (N439K, Y453F, E484K, N501Y, D614G, and P681H) described are shown as red stars. The zoom-in views of the fusion peptide in open conformation, bound compounds, putative interacting amino acid residues, and surrounding structure are shown at the right (top, dichlorcyclizine; bottom, fluoxazolevir). The zoom-in views are shown as electrostatic surface renderings using PyMOL software (blue and red surfaces indicating electropositive and electronegative surfaces).

DISCUSSION

Small-molecule antivirals can act against viral infection at multiple steps, including blocking viral entry, suppressing virally encoded enzymes, inhibiting virus assembly, or targeting a host factor required for replication (53). Small-molecule drugs also have the advantage of oral or other topical (aerosol) delivery, larger manufacturing capacity, longer shelf-life, and combination regimen. Multiple direct-acting antivirals are currently under evaluation to treat COVID-19 (54–57).

In this study, we evaluated the efficacy of previously identified small-molecule HCV fusion inhibitors (*S*)-CCZ, dichlorcyclizine, and fluoxazolevir for their efficacy against SARS-CoV-2 (14, 15, 58). While the fusion process of enveloped viruses can be grouped into three distinct classes based on the prefusion structures of their envelope proteins (types I, II, and III), the fusion-competent structures and the membrane fusion processes are quite conserved among all these viruses (16, 17). Thus, we reasoned that the above-described compounds have antiviral effects against SARS-CoV-2. Using pseudotyped viral assays, we found that these compounds are effective against SARS-CoV-2 and other highly pathogenic human CoVs with single-digit micromolar EC_{50} values in several different cell lines. Similar results were also observed in full-length infectious SARS-CoV-2 cell culture systems.

SARS-CoV-2 enters into host cells via the S glycoprotein that forms homotrimers protruding from the viral surface (6). S has two functional subunits, S1 and S2. S1 is responsible for binding to the host cell receptor (ACE2), and S2 mediates fusion of the viral and cellular membrane (6). S is cleaved at the junction between the S1 and S2 subunits, and the subsequent S2′ site is cleaved by host cell proteases such as TMPRSS2 or cathepsins (7, 8). SARS-CoV-2 is thought to enter into host cells via two distinct fusion pathways, the endosomal fusion pathway or the plasma membrane fusion pathway (7). The S2 domain, upon binding of the receptor binding domain of S1 to ACE2, undergoes conformational change and forms a fusion-competent triple helical structure that is highly conserved among most enveloped viruses (17). The hydrophobic fusion peptide then is inserted into the cellular membrane (either plasma or endosomal), bringing the cellular and viral membranes together to achieve viral fusion (17, 38, 59).

Our compounds are equally active against SARS-CoV-2-S pseudoviruses containing S protein mutations described in naturally occurring variants, including the delta variant as well as live infectious variant viruses (18–35). The Y453F mutation has been described in the SARS-CoV-2 strain infecting farmed minks and their handlers and is possibly associated with altered tropism. The N501Y and P681H mutations present in the alpha and beta variants have been linked to a more rapid spread of the virus, less susceptibility to vaccine-induced immunity, and possibly more severe disease (23). Thus, compounds targeting viral fusion (a highly conserved process), like the compounds described here, are a promising therapeutic approach against SARS-CoV-2 and emerging variants with mutations in the spike protein.

Based on the time course of compound addition and binding assays, dichlorcyclizine and fluoxazolevir do not appear to interfere with the initial attachment of virus to the cells and inhibit viral entry at a late step that is consistent with viral fusion. Cell-cell fusion assays further supported the mechanism of action of these compounds in blocking viral fusion of SARS-CoV-2, similar to the mechanism of action of these compounds in their anti-HCV activities. We recently showed that CCZ inhibits viral fusion in HCV entry by direct binding to the fusion domain of HCV envelop glycoprotein 1 (15). Fluoxazolevir has a mechanism of action similar to that of CCZ (14). By virological analyses, biochemical assays, and molecular modeling, CCZ fits into a hydrophobic pocket bordered by the putative fusion peptide of the HCV E1 protein (15). Biochemical assay with a cross-linking affinity probe and molecular modeling of CCZ and the S protein of SARS-CoV-2 demonstrate docking of the compounds into a similar structure near the fusion peptide of the S2 domain of SARS-CoV-2. Such binding may interfere with the dynamic structural changes associated with transition from prefusion to postfusion conformation. More experimental data, such as mass spectrometry, to pinpoint the binding location are necessary to validate the cross-linking and modeling results. A recent study described the development of a peptide-analog fusion inhibitor based on interaction of HR1 with HR2 of the S2 protein during the fusion process (60).

Using an *in vitro* system, we tried to select for dichlorcyclizine resistance-associated mutations but could not observe any evidence for emergence of drug resistance. It is not totally surprising that no drug-resistant isolates emerged, because the fusion mechanism and fusion peptide of the SARS-CoV-2 S protein are highly conserved. From a therapeutic perspective, it is reassuring to know that drug resistance may not be a major concern.

The anti-SARS activities of these compounds are lower (EC_{50}s about 1-log higher) than their anti-HCV activities. It is possible that the binding efficiency of these compounds to the putative binding domain of SARS-CoV-2 S protein is lower than that to the HCV E1 domain. Additional experiments are necessary to verify and characterize whether these compounds indeed bind directly to the fusion peptide or other fusion-critical sequences on the S protein of SARS-CoV-2. Future efforts to improve the efficacy of these compounds by conducting structure-activity relationship campaigns and testing in animal models will be important in developing these compounds into clinically effective drugs against COVID-19. These compounds are promising candidates for further development and could be important in stopping the spread of and treating those infected by SARS-CoV-2 and its variants as well as future emerging coronaviruses.

MATERIALS AND METHODS

Cells, chemicals, and antibodies. Huh7, Vero E6 (CRL-1586; ATCC, Manassas, VA, USA), Vero T2 (TMPRSS2-expressing cells; provided by Siyuan Ding) (61), and Vero (CCL81; ATCC) cells were cultured in Dulbecco's modified Eagle's medium (DMEM) (Corning, Corning, NY, USA). 293ACE2 cells (62) were maintained in DMEM (Corning) with 1 μg/ml puromycin. MA104 (CRL-2378.1; ATCC) and HeLa cells were grown in M199 medium (Thermo Fisher Scientific, Waltham, MA, USA) and EMEM (ATCC), respectively. Vero T2 cells were described previously (59). All media were supplemented with 10% heat-inactivated fetal bovine serum (MilliporeSigma, Burlington, MA, USA) and 1% penicillin-streptomycin (Thermo Fisher Scientific), and the cells were maintained in a 37°C and 5% CO_2 incubator.

Chemical compounds were purchased from commercial sources: remdesivir (MedKoo Biosciences, Morrisville, NC, USA), chloroquine (Key Organics, Camelford, UK), camostat (MilliporeSigma), E-64d (MilliporeSigma), and itraconazole (MilliporeSigma). (*S*)-Chlorcyclizine (CCZ) was purified from racemic chlorcyclizine (MilliporeSigma) (58). Dichlorcyclizine and fluoxazolevir were produced by American Biochemicals, Inc. (College Station, TX, USA) using synthetic protocols described previously (11–13). Antibodies against SARS-CoV-2 S protein were purchased from various commercial sources (GeneTex, Irvine, CA, USA, and Sino Biological, Chesterbrook, PA, USA) and used for controls for various virologic assays. Heparan sulfate sodium salt from porcine mucosa (MilliporeSigma) was used for the viral binding assay.

Plasmid construction. Codon-optimized SARS-CoV S (Sino Biological), SARS-CoV-2 S (GenScript, Piscataway NJ, USA), and MERS-CoV S (Sino Biological) cDNA plasmids were purchased from commercial sources. The C termini of SARS-CoV and SARS-CoV-2 S genes (containing an endoplasmic reticulum retention signal) were truncated by 20 amino acids to enhance virus yield (39, 63). A single-nucleotide mutation was introduced at nucleotide 3705 (T to A) for SARS-CoV and at nucleotide 3759 (C to A) for SARS-CoV-2 using an In-Fusion cloning kit (TaKaRa, Kusatsu, Japan) according to the manufacturer's instructions, which resulted in an amino acid change from Cys to a stop codon. For MERS-CoV, a wild-type S cDNA construct was used. In brief, pCMV-VSV-G (Addgene plasmid number 8454) (64) was digested with BamHI to remove the VSV-G sequence. The S sequences were then assembled into the cytomegalovirus promoter-containing backbone. Ten naturally occurring viral mutants (spike protein sequence mutants N439K, L452R, Y453F, S477N, E484K, N501Y, D614G, Q677H, N679S, and P681H) (18–24, 28–35) were introduced individually into the S cDNA construct by either QuikChange Lightning site-directed mutagenesis kits (Agilent Technologies, Santa Clara, CA, USA) or a Q5 site-directed mutagenesis kit (New England BioLabs, Ipswich, MA, USA). The alpha (69/70 deletion, N501Y, D614G, and P681H) (25), beta (K417N, E484K, N501Y, and D614G) (27), and delta (T19R, G142D, 156/157 deletion, R158G, L452R, T478K, D614G, P681R, and D950N) (26) variant S constructs were similarly generated. In-Fusion primer and the sequence information for SARS-CoV S, SARS-CoV-2 S, MERS-CoV S, and three SARS-CoV-2 S mutants are found in Text S1 and Tables S2 and S3 in the supplemental material. The assembled constructs were used for VSV pseudotyped virus generation.

For the cell-cell fusion assay, additional sequences were inserted into the above-described SARS-CoV-2 truncated S construct to generate truncated S-GFP and truncated S-SmBit constructs. The same BamHI-digested pCMV-VSV-G backbone was used for both constructs. For S-GFP construction, the truncated S sequence and P2A-GFP sequence were amplified by PCR and assembled with the digested backbone using the In-Fusion cloning kit according to the manufacturer's instructions. The P2A self-cleaving peptide and GFP sequences are found in Text S1. For S-SmBit construct generation, the truncated S and P2A sequences from the above-described construct were amplified by PCR and assembled as described above. Because of the short SmBit sequence, truncated S-P2A and SmBit sequences were amplified together in one reaction with a primer that includes SmBit sequence. RFP- and LgBit-expressing constructs were generated similarly. The RFP sequence and LgBit sequence from a NanoBiT PPI starter system kit (Promega, Madison, WI, USA) were amplified by PCR and assembled as described above. The RFP sequence used here is found in Text S1. For GFP-SmBit control plasmid construction, only the GFP (from the above-described S-GFP plasmid) and P2A-SmBit

(from the above-described S-SmBit plasmid) sequences were amplified by PCR and assembled into the backbone plasmid. The In-Fusion primers for generating fusion assay constructs are shown in Table S2.

SUPPLEMENTAL MATERIAL

Supplemental material is available online only.

TEXT S1, PDF file, 0.18 MB.

FIG S1, TIF file, 1.8 MB.

FIG S2, TIF file, 1.9 MB.

FIG S3, TIF file, 7.3 MB.

FIG S4, TIF file, 1.9 MB.

FIG S5, TIF file, 1.9 MB.

FIG S6, TIF file, 1.9 MB.

TABLE S1, DOCX file, 0.01 MB.

TABLE S2, DOCX file, 0.01 MB.

TABLE S3, DOCX file, 0.01 MB.

ACKNOWLEDGMENTS

This work was supported by the Intramural Research Program of the National Institute of Diabetes and Digestive and Kidney Diseases and National Center for Advancing Translational Sciences, National Institutes of Health, USA, NIH Intramural Targeted Anti-COVID-19 Program, and NIH grants K99/R00 AI135031 and R01 AI150796 and the COVID-19 Fast Grants Funding to S.D.

We thank Pei Yong Shi (UT Galveston), Theodora Hatziioannou (Rockefeller University), Ralph Baric (UNC), Bernard Lafont (NIAID), and Johnson Reed (NIAID) for sharing SARS-CoV-2 reagents.

REFERENCES

1. Gordon DE, Jang GM, Bouhaddou M, Xu J, Obernier K, White KM, O'Meara MJ, Rezelj VV, Guo JZ, Swaney DL, Tummino TA, Hüttenhain R, Kaake RM, Richards AL, Tutuncuoglu B, Foussard H, Batra J, Haas K, Modak M, Kim M, Haas P, Polacco BJ, Braberg H, Fabius JM, Eckhardt M, Soucheray M, Bennett MJ, Cakir M, McGregor MJ, Li Q, Meyer B, Roesch F, Vallet T, Mac Kain A, Miorin L, Moreno E, Naing ZZC, Zhou Y, Peng S, Shi Y, Zhang Z, Shen W, Kirby IT, Melnyk JE, Chorba JS, Lou K, Dai SA, Barrio-Hernandez I, Memon D, Hernandez-Armenta C, et al. 2020. A SARS-CoV-2 protein interaction map reveals targets for drug repurposing. Nature 583:459–468. https://doi.org/10.1038/s41586-020-2286-9.
2. Wang M, Cao R, Zhang L, Yang X, Liu J, Xu M, Shi Z, Hu Z, Zhong W, Xiao G. 2020. Remdesivir and chloroquine effectively inhibit the recently emerged novel coronavirus (2019-nCoV) in vitro. Cell Res 30:269–271. https://doi.org/10.1038/s41422-020-0282-0.
3. Sheahan TP, Sims AC, Graham RL, Menachery VD, Gralinski LE, Case JB, Leist SR, Pyrc K, Feng JY, Trantcheva I, Bannister R, Park Y, Babusis D, Clarke MO, MacKman RL, Spahn JE, Palmiotti CA, Siegel D, Ray AS, Cihlar T, Jordan R, Denison MR, Baric RS. 2017. Broad-spectrum antiviral GS-5734 inhibits both epidemic and zoonotic coronaviruses. Sci Transl Med 9:eaal3653. https://doi.org/10.1126/scitranslmed.aal3653.
4. Beigel JH, Tomashek KM, Dodd LE, Mehta AK, Zingman BS, Kalil AC, Hohmann E, Chu HY, Luetkemeyer A, Kline S, Lopez de Castilla D, Finberg RW, Dierberg K, Tapson V, Hsieh L, Patterson TF, Paredes R, Sweeney DA, Short WR, Touloumi G, Lye DC, Ohmagari N, Oh M, Ruiz-Palacios GM, Benfield T, Fätkenheuer G, Kortepeter MG, Atmar RL, Creech CB, Lundgren J, Babiker AG, Pett S, Neaton JD, Burgess TH, Bonnett T, Green M, Makowski M, Osinusi A, Nayak S, Lane HC. 2020. Remdesivir for the treatment of Covid-19—final report. N Engl J Med 383:1813–1826. https://doi.org/10.1056/NEJMoa2007764.
5. Pan H, Peto R, Henao-Restrepo A-M, Preziosi M-P, Sathiyamoorthy V, Abdool Karim Q, Alejandria MM, Hernández García C, Kieny M-P, Malekzadeh R, Murthy S, Reddy KS, Roses Periago M, Abi Hanna P, Ader F, Al-Bader AM, Alhasawi A, Allum E, Alotaibi A, Alvarez-Moreno CA, Appadoo S, Asiri A, Aukrust P, Barratt-Due A, Bellani S, Branca M, Cappel-Porter HBC, Cerrato N, Chow TS, Como N, Eustace J, García PJ, Godbole S, Gotuzzo E, Griskevicius L, Hamra R, Hassan M, Hassany M, Hutton D, Irmansyah I, Jancoriene L, Kirwan J, Kumar S, Lennon P, Lopardo G, Lydon P, Magrini N, Maguire T, Manevska S, WHO Solidarity Trial Consortium, et al. 2021. Repurposed antiviral drugs for Covid-19—interim WHO solidarity trial results. N Engl J Med 384:497–511. https://doi.org/10.1056/NEJMoa2023184.
6. Walls AC, Park YJ, Tortorici MA, Wall A, McGuire AT, Veesler D. 2020. Structure, function, and antigenicity of the SARS-CoV-2 spike glycoprotein. Cell 181:281–292.e6. https://doi.org/10.1016/j.cell.2020.02.058.
7. Tang T, Bidon M, Jaimes JA, Whittaker GR, Daniel S. 2020. Coronavirus membrane fusion mechanism offers a potential target for antiviral development. Antiviral Res 178:104792. https://doi.org/10.1016/j.antiviral.2020.104792.
8. Millet JK, Whittaker GR. 2018. Physiological and molecular triggers for SARS-CoV membrane fusion and entry into host cells. Virology 517:3–8. https://doi.org/10.1016/j.virol.2017.12.015.
9. Wang H, Yang P, Liu K, Guo F, Zhang Y, Zhang G, Jiang C. 2008. SARS coronavirus entry into host cells through a novel clathrin- and caveolae-independent endocytic pathway. Cell Res 18:290–301. https://doi.org/10.1038/cr.2008.15.
10. Hu Z, Lan KH, He S, Swaroop M, Hu X, Southall N, Zheng W, Liang TJ. 2014. Novel cell-based hepatitis C virus infection assay for quantitative high-throughput screening of anti-hepatitis C virus compounds. Antimicrob Agents Chemother 58:995–1004. https://doi.org/10.1128/AAC.02094-13.
11. He S, Xiao J, Dulcey AE, Lin B, Rolt A, Hu Z, Hu X, Wang AQ, Xu X, Southall N, Ferrer M, Zheng W, Liang TJ, Marugan JJ. 2016. Discovery, optimization, and characterization of novel chlorcyclizine derivatives for the treatment of hepatitis C virus infection. J Med Chem 59:841–853. https://doi.org/10.1021/acs.jmedchem.5b00752.
12. He S, Li K, Lin B, Hu Z, Xiao J, Hu X, Wang AQ, Xu X, Ferrer M, Southall N, Zheng W, Schoenen FJ, Marugan JJ, Liang TJ, Frankowski KJ, Aubé J, Schoenen FJ, Marugan JJ, Liang TJ, Frankowski KJ. 2017. Development of an aryloxazole class of hepatitis C virus inhibitors targeting the entry stage of the viral replication cycle. J Med Chem 60:6364–6383. https://doi.org/10.1021/acs.jmedchem.7b00561.
13. Rolt A, Le D, Hu Z, Wang AQ, Shah P, Singleton M, Hughes E, Dulcey AE, He S, Imamura M, Uchida T, Chayama K, Xu X, Marugan JJ, Liang TJ. 2018. Preclinical pharmacological development of chlorcyclizine derivatives for the treatment of hepatitis C virus infection. J Infect Dis 217:1761–1769. https://doi.org/10.1093/infdis/jiy039.
14. Ma CD, Imamura M, Talley DC, Rolt A, Xu X, Wang AQ, Le D, Uchida T, Osawa M, Teraoka Y, Li K, Hu X, Park SB, Chalasani N, Irvin PH, Dulcey AE, Southall N, Marugan JJ, Hu Z, Chayama K, Frankowski KJ, Liang TJ. 2020.

Fluoxazolevir inhibits hepatitis C virus infection in humanized chimeric mice by blocking viral membrane fusion. Nat Microbiol 5:1532–1541. https://doi.org/10.1038/s41564-020-0781-2.
15. Hu Z, Rolt A, Hu X, Ma CD, Le DJ, Park SB, Houghton M, Southall N, Anderson DE, Talley DC, Lloyd JR, Marugan JC, Liang TJ. 2020. Chlorcyclizine inhibits viral fusion of hepatitis C virus entry by directly targeting HCV envelope glycoprotein 1. Cell Chem Biol 27:780–792.e5. https://doi.org/10.1016/j.chembiol.2020.04.006.
16. Harrison SC. 2015. Viral membrane fusion. Virology 479–480:498–507. https://doi.org/10.1016/j.virol.2015.03.043.
17. White JM, Whittaker GR. 2016. Fusion of enveloped viruses in endosomes. Traffic 17:593–614. https://doi.org/10.1111/tra.12389.
18. Kymie C, Nonaka V, Franco MMM, Gräf T, Verena A, Mendes AAVA, Santana De Aguiar R, Giovanetti M, Solano B, Souza F, Souza B, Nonaka CKV, Franco MMM, Gräf T, De Lorenzo Barcia CA, De Ávila Mendonça RN, De Sousa KAF, Costa Neiva LM, Fosenca V, Mendes AAVA, De Aguiar RS, Giovanetti M, De Freitas Souza BS, Kymie C, Nonaka V, Franco MMM, Gräf T, Verena A, Mendes AAVA, Santana De Aguiar R, Giovanetti M, Solano B, Souza F, Souza B. 2021. Genomic evidence of a SARs-Cov-2 reinfection case with E484K spike mutation in Brazil. Emerg Infect Dis 27:1522–1524. https://doi.org/10.3201/eid2705.210191.
19. Bayarri-Olmos R, Rosbjerg A, Johnsen LB, Helgstrand C, Bak-Thomsen T, Garred P. 2021. The SARS-CoV-2 Y453F mink variant displays a striking increase in ACE-2 affinity but does not challenge antibody neutralization. J Biol Chem 296:100536. https://doi.org/10.1016/j.jbc.2021.100536.
20. Albulescu IC, Kovacikova K, Tas A, Snijder EJ, van Hemert MJ, Otero A, Carballido JL, Salgado L, Canudo JI, Garrido C, Kecerdasan I, Ikep P, Clausen TM, Sandoval DR, Spliid CB, Pihl J, Perrett HR, Painter CD, Narayanan A, Majowicz SA, Kwong EM, McVicar RN, Thacker BE, Glass CA, Yang Z, Torres JL, Golden GJ, Bartels PL, Porell RN, Garretson AF, Laubach L, Feldman J, Yin X, Pu Y, Hauser BM, Caradonna TM, Kellman BP, Martino C, Gordts PLSM, Chanda SK, Schmidt AG, Godula K, Leibel SL, Jose J, Corbett KD, Ward AB, Carlin AF, Esko JD, Walls AC, Xiong X, Park YJ, Tortorici MA, Snijder J, et al. 2021. Genetic characteristics and phylogeny of 969-bp S gene sequence of SARS-CoV-2 from Hawaii reveals the worldwide emerging P681H mutation. Hawai'i J Heal Soc Welf 80:52–61.
21. Harrison AG, Lin T, Wang P. 2020. Mechanisms of SARS-CoV-2 transmission and pathogenesis. Trends Immunol 41:1100–1115. https://doi.org/10.1016/j.it.2020.10.004.
22. Liu Z, VanBlargan LA, Bloyet LM, Rothlauf PW, Chen RE, Stumpf S, Zhao H, Errico JM, Theel ES, Liebeskind MJ, Alford B, Buchser WJ, Ellebedy AH, Fremont DH, Diamond MS, Whelan SPJ. 2021. Identification of SARS-CoV-2 spike mutations that attenuate monoclonal and serum antibody neutralization. Cell Host Microbe 29:477–488. https://doi.org/10.1016/j.chom.2021.01.014.
23. Leung K, Shum MH, Leung GM, Lam TT, Wu JT. 2021. Early transmissibility assessment of the N501Y mutant strains of SARS-CoV-2 in the United Kingdom, October to November 2020. Eurosurveillance 26. https://doi.org/10.2807/1560-7917.ES.2020.26.1.2002106.
24. Jaimes JA, André NM, Chappie JS, Millet JK, Whittaker GR. 2020. Phylogenetic analysis and structural modeling of SARS-CoV-2 spike protein reveals an evolutionary distinct and proteolytically sensitive activation loop. J Mol Biol 432:3309–3325. https://doi.org/10.1016/j.jmb.2020.04.009.
25. Meng B, Kemp SA, Papa G, Datir R, Ferreira IATM, Marelli S, Harvey WT, Lytras S, Mohamed A, Gallo G, Thakur N, Collier DA, Mlcochova P, Robson SC, Loman NJ, Connor TR, Golubchik T, Martinez Nunez RT, Ludden C, Corden S, Johnston I, Bonsall D, Smith CP, Awan AR, Bucca G, Torok ME, Saeed K, Prieto JA, Jackson DK, Hamilton WL, Snell LB, Moore C, Harrison EM, Goncalves S, Fairley DJ, Loose MW, Watkins J, Livett R, Moses S, Amato R, Nicholls S, Bull M, Smith DL, Barrett J, Aanensen DM, Curran MD, Parmar S, Aggarwal D, Shepherd JG, Parker MD, et al. 2021. Recurrent emergence of SARS-CoV-2 spike deletion H69/V70 and its role in the alpha variant B.1.1.7. Cell Rep 35:109292. https://doi.org/10.1016/j.celrep.2021.109292.
26. Planas D, Veyer D, Baidaliuk A, Staropoli I, Guivel-Benhassine F, Rajah MM, Planchais C, Porrot F, Robillard N, Puech J, Prot M, Gallais F, Gantner P, Velay A, Le Guen J, Kassis-Chikhani N, Edriss D, Belec L, Seve A, Courtellemont L, Péré H, Hocqueloux L, Fafi-Kremer S, Prazuck T, Mouquet H, Bruel T, Simon-Lorière E, Rey FA, Schwartz O. 2021. Reduced sensitivity of SARS-CoV-2 variant delta to antibody neutralization. Nature 596:276–280. https://doi.org/10.1038/s41586-021-03777-9.
27. Villoutreix BO, Calvez V, Marcelin AG, Khatib AM. 2021. In silico investigation of the new UK (B.1.1.7) and South African (501y.v2) SARS-CoV-2 variants with a focus at the ace2–spike rbd interface. Int J Mol Sci 22:1695. https://doi.org/10.3390/ijms22041695.
28. Thomson EC, Rosen LE, Shepherd JG, Spreafico R, Filipe S, Wojcechowskyj JA, Davis C, Piccoli L, David J, Dillen J, Lytras S, Czudnochowski N, Shah R, Jesudason N, De Marco A, Li K, Bassi J, Toole AO, Pinto D, Colquhoun RM, Culap K, Jackson B, Zatta F, Rambaut A, Jaconi S, Sreenu VB, Nix J, Zhang I, Ruth F, Glass WG, Beltramello M, Nomikou K, Pizzuto M, Cameroni E, Croll TI, Johnson N, Iulio J, Di Ceschi A, Harbison AM, Mair D, Ferrari P, Smollett K, Sallusto F, Carmichael S, Garzoni C, Galli M, Hughes J, Riva A, Ho A, Schiuma M, COVID-19 Genomics UK (COG-UK) Consortium, et al. 2021. Circulating SARS-CoV-2 spike N439K variants maintain fitness while evading antibody-mediated immunity. Cell 184:1171–1187. https://doi.org/10.1016/j.cell.2021.01.037.
29. Deng X, Garcia-Knight MA, Khalid MM, Servellita V, Wang C, Morris MK, Sotomayor-González A, Glasner DR, Reyes KR, Gliwa AS, Reddy NP, Sanchez San Martin C, Federman S, Cheng J, Balcerek J, Taylor J, Streithorst JA, Miller S, Sreekumar B, Chen PY, Schulze-Gahmen U, Taha TY, Hayashi JM, Simoneau CR, Kumar GR, McMahon S, Lidsky PV, Xiao Y, Hemarajata P, Green NM, Espinosa A, Kath C, Haw M, Bell J, Hacker JK, Hanson C, Wadford DA, Anaya C, Ferguson D, Frankino PA, Shivram H, Lareau LF, Wyman SK, Ott M, Andino R, Chiu CY. 2021. Transmission, infectivity, and neutralization of a spike L452R SARS-CoV-2 variant. Cell 184:3426–3437.e8. https://doi.org/10.1016/j.cell.2021.04.025.
30. Daniloski Z, Jordan TX, Ilmain JK, Guo X, Bhabha G, TenOever BR, Sanjana NE. 2021. The Spike D614G mutation increases SARS-CoV-2 infection of multiple human cell types. Elife 2021:e65365. https://doi.org/10.7554/eLife.65365.
31. Korber B, Fischer WM, Gnanakaran S, Yoon H, Theiler J, Abfalterer W, Hengartner N, Giorgi EE, Bhattacharya T, Foley B, Hastie KM, Parker MD, Partridge DG, Evans CM, Freeman TM, de Silva TI, Angyal A, Brown RL, Carrilero L, Green LR, Groves DC, Johnson KJ, Keeley AJ, Lindsey BB, Parsons PJ, Raza M, Rowland-Jones S, Smith N, Tucker RM, Wang D, Wyles MD, McDanal C, Perez LG, Tang H, Moon-Walker A, Whelan SP, LaBranche CC, Saphire EO, Montefiori DC, Sheffield COVID-19 Genomics Group. 2020. Tracking changes in SARS-CoV-2 Spike: evidence that D614G increases infectivity of the COVID-19 virus. Cell 182:812–827. https://doi.org/10.1016/j.cell.2020.06.043.
32. Zhang L, Jackson CB, Mou H, Ojha A, Peng H, Quinlan BD, Rangarajan ES, Pan A, Vanderheiden A, Suthar MS, Li W, Izard T, Rader C, Farzan M, Choe H. 2020. SARS-CoV-2 spike-protein D614G mutation increases virion spike density and infectivity. Nat Commun 11:1–9. https://doi.org/10.1038/s41467-020-19808-4.
33. LoTempio J, Billings E, Draper K, Ralph C, Moshgriz M, Duong N, Bard JD, Gai X, Wessel D, DeBiasi RL, Campos JM, Vilain E, Delaney M, Michael DG. 2021. Novel SARS-CoV-2 spike variant identified through viral genome sequencing of the pediatric Washington D.C. COVID-19 outbreak. medRxiv https://doi.org/10.1101/2021.02.08.21251344.
34. Yurkovetskiy L, Wang X, Pascal KE, Tomkins-Tinch C, Nyalile TP, Wang Y, Baum A, Diehl WE, Dauphin A, Carbone C, Veinotte K, Egri SB, Schaffner SF, Lemieux JE, Munro JB, Rafique A, Barve A, Sabeti PC, Kyratsous CA, Dudkina NV, Shen K, Luban J. 2020. Structural and functional analysis of the D614G SARS-CoV-2 spike protein variant. Cell 183:739–751. https://doi.org/10.1016/j.cell.2020.09.032.
35. Grabowski F, Preibisch G, Giziński S, Kochańczyk M, Lipniacki T. 2021. SARS-COV-2 variant of concern 202012/01 has about twofold replicative advantage and acquires concerning mutations. Viruses 13:392–396. https://doi.org/10.3390/v13030392.
36. Kandimalla KK, Donovan MD. 2005. Carrier mediated transport of chlorpheniramine and chlorcyclizine across bovine olfactory mucosa: implications on nose-to-brain transport. J Pharm Sci 94:613–624. https://doi.org/10.1002/jps.20284.
37. Savarino A, Boelaert JR, Cassone A, Majori G, Cauda R. 2003. Effects of chloroquine on viral infections: an old drug against today's diseases? Lancet Infect Dis 3:722–727. https://doi.org/10.1016/S1473-3099(03)00806-5.
38. Hoffmann M, Kleine-Weber H, Schroeder S, Krüger N, Herrler T, Erichsen S, Schiergens TS, Herrler G, Wu NH, Nitsche A, Müller MA, Drosten C, Pöhlmann S. 2020. SARS-CoV-2 cell entry depends on ACE2 and TMPRSS2 and is blocked by a clinically proven protease inhibitor. Cell 181:271–280. https://doi.org/10.1016/j.cell.2020.02.052.
39. Case JB, Rothlauf PW, Chen RE, Liu Z, Zhao H, Kim AS, Bloyet LM, Zeng Q, Tahan S, Droit L, Ilagan MXG, Tartell MA, Amarasinghe G, Henderson JP, Miersch S, Ustav M, Sidhu S, Virgin HW, Wang D, Ding S, Corti D, Theel ES, Fremont DH, Diamond MS, Whelan SPJ. 2020. Neutralizing antibody and soluble ACE2 inhibition of a replication-competent VSV-SARS-CoV-2 and a clinical isolate of SARS-CoV-2. Cell Host Microbe 28:475–485. https://doi.org/10.1016/j.chom.2020.06.021.
40. Wang N, Shi X, Jiang L, Zhang S, Wang D, Tong P, Guo D, Fu L, Cui Y, Liu X, Arledge KC, Chen YH, Zhang L, Wang X. 2013. Structure of MERS-CoV spike receptor-binding domain complexed with human receptor DPP4. Cell Res 23:986–993. https://doi.org/10.1038/cr.2013.92.
41. Xie X, Muruato A, Lokugamage KG, Narayanan K, Zhang X, Zou J, Liu J, Schindewolf C, Bopp NE, Aguilar PV, Plante KS, Weaver SC, Makino S, LeDuc

JW, Menachery VD, Shi PY. 2020. An infectious cDNA clone of SARS-CoV-2. Cell Host Microbe 27:841–848. https://doi.org/10.1016/j.chom.2020.04.004.
42. Clausen TM, Sandoval DR, Spliid CB, Pihl J, Perrett HR, Painter CD, Narayanan A, Majowicz SA, Kwong EM, McVicar RN, Thacker BE, Glass CA, Yang Z, Torres JL, Golden GJ, Bartels PL, Porell RN, Garretson AF, Laubach L, Feldman J, Yin X, Pu Y, Hauser BM, Caradonna TM, Kellman BP, Martino C, Gordts PLSM, Chanda SK, Schmidt AG, Godula K, Leibel SL, Jose J, Corbett KD, Ward AB, Carlin AF, Esko JD. 2020. SARS-CoV-2 infection depends on cellular heparan sulfate and ACE2. Cell 183:1043–1057. https://doi.org/10.1016/j.cell.2020.09.033.
43. Kim SY, Jin W, Sood A, Montgomery DW, Grant OC, Fuster MM, Fu L, Dordick JS, Woods RJ, Zhang F. 2020. Characterization of heparin and severe acute respiratory syndrome-related coronavirus 2 (SARS-CoV-2) spike glycoprotein binding interactions. Antiviral Res 181:104873. https://doi.org/10.1016/j.antiviral.2020.104873.
44. Murray EJ, Grisanti MS, Bentley GV, Murray SS. 1997. E64d, a membrane-permeable cysteine protease inhibitor, attenuates the effects of parathyroid hormone on osteoblasts in vitro. Metabolism 46:1090–1094. https://doi.org/10.1016/S0026-0495(97)90284-5.
45. Zhang R, Li Y, Zhang AL, Wang Y, Molina MJ. 2020. Erratum: identifying airborne transmission as the dominant route for the spread of COVID-19. Proc Natl Acad Sci U S A 117:14857–14863. https://doi.org/10.1073/pnas.2009637117.
46. Trinh MN, Lu F, Li X, Das A, Liang Q, De Brabander JK, Brown MS, Goldstein JL. 2017. Triazoles inhibit cholesterol export from lysosomes by binding to NPC1. Proc Natl Acad Sci U S A 114:89–94. https://doi.org/10.1073/pnas.1619571114.
47. Greaney AJ, Loes AN, Crawford KHD, Starr TN, Malone KD, Chu HY, Bloom JD. 2021. Comprehensive mapping of mutations in the SARS-CoV-2 receptor-binding domain that affect recognition by polyclonal human plasma antibodies. Cell Host Microbe 29:463–476. https://doi.org/10.1016/j.chom.2021.02.003.
48. Greaney AJ, Starr TN, Gilchuk P, Zost SJ, Binshtein E, Loes AN, Hilton SK, Huddleston J, Eguia R, Crawford KHD, Dingens AS, Nargi RS, Sutton RE, Suryadevara N, Rothlauf PW, Liu Z, Whelan SPJ, Carnahan RH, Crowe JE, Bloom JD. 2021. Complete mapping of mutations to the SARS-CoV-2 spike receptor-binding domain that escape antibody recognition. Cell Host Microbe 29:44–57. https://doi.org/10.1016/j.chom.2020.11.007.
49. Starr TN, Greaney AJ, Addetia A, Hannon WW, Choudhary MC, Dingens AS, Li JZ, Bloom JD. 2021. Prospective mapping of viral mutations that escape antibodies used to treat COVID-19. Science 371:850–854. https://doi.org/10.1126/science.abf9302.
50. Weisblum Y, Schmidt F, Zhang F, DaSilva J, Poston D, Lorenzi JCC, Muecksch F, Rutkowska M, Hoffmann HH, Michailidis E, Gaebler C, Agudelo M, Cho A, Wang Z, Gazumyan A, Cipolla M, Luchsinger L, Hillyer CD, Caskey M, Robbiani DF, Rice CM, Nussenzweig MC, Hatziioannou T, Bieniasz PD. 2020. Escape from neutralizing antibodies 1 by SARS-CoV-2 spike protein variants. Elife 9:1. https://doi.org/10.7554/eLife.61312.
51. Cai Y, Zhang J, Xiao T, Peng H, Sterling SM, Walsh RM, Rawson S, Rits-Volloch S, Chen B. 2020. Distinct conformational states of SARS-CoV-2 spike protein. Science 369:1586–1592. https://doi.org/10.1126/science.abd4251.
52. Wrapp D, Wang N, Corbett KS, Goldsmith JA, Hsieh CL, Abiona O, Graham BS, McLellan JS. 2020. Cryo-EM structure of the 2019-nCoV spike in the prefusion conformation. Science 367:1260–1263. https://doi.org/10.1126/science.abb2507.
53. Zumla A, Chan JFW, Azhar EI, Hui DSC, Yuen KY. 2016. Coronaviruses-drug discovery and therapeutic options. Nat Rev Drug Discov 15:327–347. https://doi.org/10.1038/nrd.2015.37.
54. Choudhary S, Sharma K, Silakari O. 2021. The interplay between inflammatory pathways and COVID-19: a critical review on pathogenesis and therapeutic options. Microb Pathog 150:104673. https://doi.org/10.1016/j.micpath.2020.104673.
55. Wang M-Y, Zhao R, Gao L-J, Gao X-F, Wang D-P, Cao J-M. 2020. SARS-CoV-2: structure, biology, and structure-based therapeutics development. Front Cell Infect Microbiol 10:587269. https://doi.org/10.3389/fcimb.2020.587269.
56. Bolarin J, Oluwatoyosi M, Orege J, Emmanuel A, Ibrahim Y, Adeyemi S. 2021. Therapeutic drugs for SARS-CoV-2 treatment: current state and perspective. Int Immunopharmacol 90:107228. https://doi.org/10.1016/j.intimp.2020.107228.
57. Al Adem K, Shanti A, Stefanini C, Lee S. 2020. Inhibition of SARS-COV-2 entry into host cells using small molecules. Pharmaceuticals 13:447–454. https://doi.org/10.3390/ph13120447.
58. He S, Lin B, Chu V, Hu Z, Hu X, Xiao J, Wang AQ, Schweitzer CJ, Li Q, Imamura M, Hiraga N, Southall N, Ferrer M, Zheng W, Chayama K, Marugan JJ, Liang TJ. 2015. Repurposing of the antihistamine chlorcyclizine and related compounds for treatment of hepatitis C virus infection. Sci Transl Med 7:282ra49. https://doi.org/10.1126/scitranslmed.3010286.
59. Matsuyama S, Nao N, Shirato K, Kawase M, Saito S, Takayama I, Nagata N, Sekizuka T, Katoh H, Kato F, Sakata M, Tahara M, Kutsuna S, Ohmagari N, Kuroda M, Suzuki T, Kageyama T, Takeda M. 2020. Enhanced isolation of SARS-CoV-2 by TMPRSS2-expressing cells. Proc Natl Acad Sci U S A 117:7001–7003. https://doi.org/10.1073/pnas.2002589117.
60. Xia S, Liu M, Wang C, Xu W, Lan Q, Feng S, Qi F, Bao L, Du L, Liu S, Qin C, Sun F, Shi Z, Zhu Y, Jiang S, Lu L. 2020. Inhibition of SARS-CoV-2 (previously 2019-nCoV) infection by a highly potent pan-coronavirus fusion inhibitor targeting its spike protein that harbors a high capacity to mediate membrane fusion. Cell Res 30:343–355. https://doi.org/10.1038/s41422-020-0305-x.
61. Zang R, Case JB, Yutuc E, Ma X, Shen S, Castro MFG, Liu Z, Zeng Q, Zhao H, Son J, Rothlauf PW, Kreutzberger AJB, Hou G, Zhang H, Bose S, Wang X, Vahey MD, Mani K, Griffiths WJ, Kirchhausen T, Fremont DH, Guo H, Diwan A, Wang Y, Diamond MS, Whelan SPJ, Ding S. 2020. Cholesterol 25-hydroxylase suppresses SARS-CoV-2 replication by blocking membrane fusion. Proc Natl Acad Sci U S A 117:32105–32113. https://doi.org/10.1073/pnas.2012197117.
62. Zhang Q, Chen CZ, Swaroop M, Xu M, Wang L, Lee J, Wang AQ, Pradhan M, Hagen N, Chen L, Shen M, Luo Z, Xu X, Xu Y, Huang W, Zheng W, Ye Y. 2020. Heparan sulfate assists SARS-CoV-2 in cell entry and can be targeted by approved drugs in vitro. Cell Discov https://doi.org/10.1038/s41421-020-00222-5.
63. Xiong HL, Wu YT, Cao JL, Yang R, Liu YX, Ma J, Qiao XY, Yao XY, Zhang BH, Zhang YL, Hou WH, Shi Y, Xu JJ, Zhang L, Wang SJ, Fu BR, Yang T, Ge SX, Zhang J, Yuan Q, Huang BY, Li ZY, Zhang TY, Xia NS. 2020. Robust neutralization assay based on SARS-CoV-2 S-protein-bearing vesicular stomatitis virus (VSV) pseudovirus and ACE2-overexpressing BHK21 cells. Emerg Microbes Infect 9:2105–2113. https://doi.org/10.1080/22221751.2020.1815589.
64. Stewart SA, Dykxhoorn DM, Palliser D, Mizuno H, Yu EY, An DS, Sabatini DM, Chen ISY, Hahn WC, Sharp PA, Weinberg RA, Novina CD. 2003. Lentivirus-delivered stable gene silencing by RNAi in primary cells. RNA 9:493–501. https://doi.org/10.1261/rna.2192803.